Mass-Ablation Rates in a Spherical Laser-Produced Plasma

J. A. Tarvin, W. B. Fechner, J. T. Larsen, P. D. Rockett, and D. C. Slater
KMS Fusion, Inc., Ann Arbor, Michigan 48106
(Received 3 February 1983)

Measurements of the rate at which 1.05-μm light ablates material from spherical targets are reported for absorbed intensities between 4×10^{13} and 4×10^{14} W/cm^2. At 4×10^{14}, the ablation rate is twice as high as has been reported for planar targets. A steady-state model which includes inhibited thermal transport matches the data well.

PACS numbers: 52.25.Pd, 52.25.Fi, 52.50.Jm

A major factor affecting the performance of a laser-fusion target is the efficiency with which absorbed energy is converted to kinetic energy of implosion. That efficiency is determined by the transport of energy from the absorption region to more dense material, where the driving pressure for the implosion is developed.[1]

Many experiments[2,3] have indicated that electron thermal transport is less efficient in laser-produced plasmas than the standard diffusion treatment[4] indicates. Such experiments are usually modeled by placing an upper limit on the thermal flux, so that the flux is given by the smaller of the diffusive flux, $\kappa\nabla T$, and the limited free-streaming flux, $fnkT(kT/m)^{1/2}\nabla T/|\nabla T|$. Here, κ is the Spitzer conductivity[4]; n,T, and m are the electron number density, temperature, and mass, respectively; and f is a dimensionless number, referred to as the flux limiter. Experiments typically require $f=0.03$ when the absorbed intensity reaches 10^{14} W/cm^2. Recent theoretical work[5] supports some limitation of thermal flux but suggests that a more sophisticated treatment is required. In the intensity regime where flux limiting is usually applied, resonance absorption of laser light can generate a suprathermal electron population, which may require a different transport treatment.

A number of experiments[6-11] have been performed to study thermal transport. However, no experiment has measured thermal transport directly because the densities, temperatures, and temperature gradients in laser plasmas are too great to be controlled independently. So the experiments have concentrated on measuring the rate, $\dot{m}$, at which light ablates material from a unit area of a target. The ablation rate is closely related to thermal transport because it is a measure of the depth of material penetrated by the heat front during the laser pulse. Most ablation measurements have been made with planar targets, for which analytical and computational models must take account of lateral transport, lateral plasma flow, and target-edge effects. The complications are greatest at high intensity because the size of the illuminated region is limited by the available laser power. For spherical target experiments,[10,11] lateral transport and flow smooth inhomogeneities and enhance the spherical symmetry, making the hydrodynamics more nearly one dimensional.

In this Letter, we report mass-ablation rates for spherical targets determined from time-resolved x-ray measurements. The incident wavelength, λ, was 1.05 μm and the absorbed intensity varied from 4×10^{13} to 4×10^{14} W/cm^2. At the lower intensities, the data are reasonably consistent with the ablation rates observed in the spherical-target experiment by Goldsack *et al.*[10] and with ablation rates observed from planar targets.[9] At high intensity, however, $\dot{m}$ is twice as large as has been reported for planar targets. The new data are represented well by a stead-state analytical model,[12] which is based on flux-limited thermal transport.

The laser pulse used in this experiment was constructed by combining ten 100-psec pulses[13] with a delay of 100 psec between pulses. The pulse was 950 psec wide at half maximum and the rise time from 10% to 80% of peak power was 90 psec. The power was nearly constant during the central 850 psec of the pulse. This pulse shape delivers no more than 5% of the laser energy at less than half power. The two beams of the laser were focused on opposite sides of the target by an all-reflective optical system.[14] Each beam, which filled a 144-deg cone, was focused 0.15 diameter beyond target center so that the entire target surface was illuminated. This offset was found empirically to optimize the symmetry both of holographic interferograms[15] of the underdense plasma and of the imploding cores of thin-walled targets.[14] The maximum angle of incidence, θ_i, in this geometry is 18°. So the turning point of the laser light is at $\cos^2\theta_i n_c = 0.88 n_c$, where n_c is the critical density, $\pi mc^2/\lambda^2e^2$. Because the

illumination is near normal, refractive effects are minor.

The targets were spherical glass shells 6 μm thick which were coated, in order, with 0.5 μm aluminum, 0.5–7.0 μm parylene (C_8H_8), and 0.01 μm titanium. The outer diameter of the targets ranged from 73 to 105 μm. The multiple layers of the targets were designed for use with an x-ray streak camera. The thin Ti layer emits a short burst of x rays which mark the onset of the laser pulse. Parylene emits relatively few x rays, so that the increased emission from Al gives a clear signature when the parylene has been completely ablated. The streak camera was used with a pinhole, which attenuated the x-ray flux and provided spatial resolution. The camera was normal to the (horizontal) laser axis and 45 deg from the (vertical) target support stalk. The 100-nm CsI photocathode was oriented to view the equator of the target, where the two laser beams overlap. The photocathode substrate was a 300-nm carbon foil coated with 25 nm of Au. A 25-μm Be filter provided a low-energy cutoff of approximately 1 keV.

Other target diagnostics included differential plasma calorimeters[16] to measure the absorbed energy, pulsed interferometric holography to measure the instantaneous plasma profile, measurements of the hard-x-ray spectrum, and the time dependence of the spectrum of light reflected from the target. The fraction of incident energy absorbed is $(31\pm5)\%$, and is independent of incident intensity. The hard-x-ray spectrum and fast-ion measurements indicate that half to three-quarters of the absorbed energy appears in suprathermal electrons with a characteristic temperature varying from 4.5 ± 1 keV at 4×10^{13} W/cm^2 absorbed to 10 ± 3 keV at 4×10^{14} W/cm^2. The presence of suprathermal electrons and the weak dependence of absorption on intensity are both characteristic of resonance absorption.

The streak photograph from a target with 4×10^{14} W/cm^2 absorbed is shown in Fig. 1. The burst from the Ti layer is less than 50 psec long and emission from the parylene is weak. The photograph is not symmetric from top to bottom because the bottom of the target is obscured by the target stalk. In the analysis of the data, only the top of the image is used. The aluminum x-ray emission first occurs near the original target diameter, where it is enhanced by limb brightening. As the aluminum moves out into the corona, the emission inside the target diameter becomes more visible because the optically thin Al

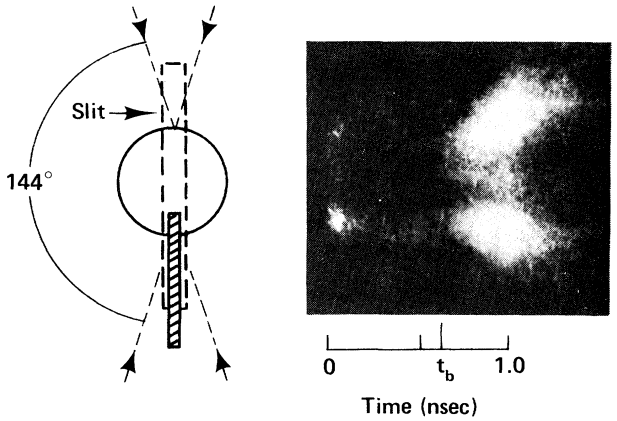

FIG. 1. X-ray streak photograph, showing the rapid increase of emission when the parylene has been ablated and the Al layer is heated. Note the short burst of x rays from the Ti layer, which marks the onset of the laser pulse. The sketch shows the target image produced by the pinhole camera superimposed on the slit-like photocathode. The marginal rays of the two 144° cones of laser light are also shown.

plasma grows thicker. Thus, the first appearance of the Al emission is the signature of the burnthrough time, t_b.

To calculate $\dot{m}$ from the measured burnthrough time, the area of the ablation surface must be known. However, the ablation surface is difficult to observe. It is too dense to be probed by UV holography, but not hot enough to be visible in x-ray emission. Figure 1 shows that material at the original target diameter is hot enough to emit 1-keV x rays throughout the entire laser pulse, and so the (cold) ablation surface must lie inside the original target diameter. We make the conservative estimate that the ablation surface is the same as the initial target surface. In that case, the ablation rate is given by

$$\dot{m}=\rho_p d_p/t_b, \tag{1}$$

where ρ_p and d_p are the initial density (1.1 g/cm^3) and thickness of the parylene layer, respectively. Equation (1) underestimates $\dot{m}$ late in the pulse, because ablated Al is observed only when it is hot enough to radiate. However, $\dot{m}$ is greater than average before steady state is reached. These two effects are linked because the time required to reach steady state is related to the time required to transport material from the ablation surface to the critical surface, where the Al is hot enough to radiate. Computer simulations of this experiment[15] show that each effect is equivalent to changing t_b by about 150 psec but that they

approximately cancel one another. So Eq. (1) provides an accurate estimate of the steady-state ablation rate.

The ablation rate obtained from the burnthrough measurements is compared with data from planar and spherical targets in Fig. 2, where the absorbed intensity, I_{abs}, is the measured absorbed energy divided by the measured pulse length and the initial target surface area. Below 4×10^{13} W/cm^2, the planar-target data[9] are similar to ion data from spherical targets,[10] although there is a small systematic discrepancy. The present data lie ~25% below the ion data of Goldsack *et al.*[10] in the small region of overlap. At the highest intensities, the ablation rate from spherical targets is twice as large as what has been reported for planar targets.[6,8,10] The different geometries lead to different ablation rates, complicating the interpretation of transport properties.

The steady-state theory of spherical ablation developed by Max, McKee, and Mead[12] provides a basis for interpretation of our results. The model includes inhibited thermal transport (using a flux limit parameter) and assumes that the absorbed energy is deposited with thermal electrons at the critical surface.

Density profiles obtained from interferometric holograms[15] and measurements of the critical surface velocity[3,15] show that a stationary profile is achieved after the first 300 psec of the event. These measurements of the underdense ($n \leq n_c$) plasma indicate that the overdense ($n \geq n_c$) plasma reaches steady state early in the laser pulse, as the model assumes.

The suprathermal electrons present in this experiment have two potential effects. First, since the suprathermal electrons have long mean free paths, they deposit some of their energy in overdense plasma. Consequently, the flux limit parameter that fits the data best will overestimate the energy transport (by thermal electrons) inward from critical and will, therefore, provide an upper limit for the flux limiter that would be required if thermal and suprathermal groups were treated separately in the model. Second, the fast electrons decouple some energy from the dense material by accelerating ions in the low-density corona of the target. An upper limit for the effect of fast-ion losses is obtained by reducing the nominal intensity associated with a data point by the fast-ion fraction observed for that intensity. Fast-ion measurements reported for a previous experiment with similar laser and target parameters[17] indicate that the correction to

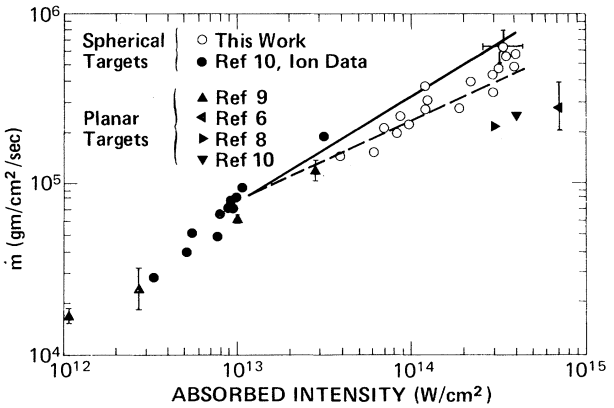

FIG. 2. Mass-ablation rate vs absorbed intensity for $\lambda = 1.05\ \mu$m. Curves are from the model of Ref. 12. Solid line, $f = 0.25$; dashed line, $f = 0.03$.

I_{abs} would vary from 15% at 10^{14} W/cm^2 to 30% at 4×10^{14} W/cm^2.

When I_{abs} is high enough for transport to be inhibited, the model gives an ablation rate of the form

$$\dot{m} = A\left(\frac{I_{abs}}{10^{14}\ \mathrm{W/cm^2}}\right)^{\alpha}\left(\frac{\lambda}{1\ \mu\mathrm{m}}\right)^{\beta}\left(\frac{R_a}{50\ \mu\mathrm{m}}\right)^{\gamma}, \quad (2)$$

where R_a is the radius of the ablation surface. The coefficient A and the exponents α, β, and γ depend on the flux limiter. A is most sensitive to f when f is small and the exponents are most sensitive when f is large. For 1-μm light and 100-μm-diam targets, the ablation rate curves for $f \geq 0.03$ intersect when I_{abs} is between 10^{13} and 3×10^{13} W/cm^2. So, unless f is less than 0.03, transport inhibition is only important at higher intensities.

The ablation rate from Max, McKee, and Mead[12] is shown for two values of f in Fig. 2. While a flux limiter of 0.04 would fit our data best, anything between 0.03 and 0.10 would be reasonably consistent with the data. A correction for fast-ion losses would change the best fit to $f = 0.06$. In spite of the reservations concerning its applicability, the model reproduces the data well.

The interpretation of the present experiment differs from those of Ref. 10, which required a flux limiter greater than 0.1, and Ref. 11, which was inconsistent with flux-limited transport. The differences in the experiments relate primarily to the absorption modeling. Because of the illumination geometry, much of the absorption in Ref. 10 is expected at subcritical densities. The targets in Ref. 11 are much larger, leading to longer scale lengths, and less resonance absorp-

tion than in the experiments presented here. Until a better theoretical understanding of energy transport in laser-produced plasma is available, it will be difficult to reconcile the results of experiments which appear rather similar but which lead to very different conclusions.

In summary, the present experiment shows mass-ablation rates higher than planar-target experiments have at absorbed intensities above 10^{14} W/cm^2. The steady-state model of Max, McKee, and Mead matches the data well with a flux limiter of 0.03–0.10. The degree of flux limiting differs from that deduced from other recent spherical-target experiments.

We are grateful to D. Attwood and the laser program at Lawrence Livermore National Laboratory for the generous loan of an x-ray streak camera, without which this experiment would not have been possible. We are also grateful to H. Medecki for his technical assistance. This work was supported by the U. S. Department of Energy under Contract No. DE-AC08-82DP40152.

[1]K. A. Brueckner and S. Jorna, Rev. Mod. Phys. 46, 325 (1974).

[2]R. C. Malone, R. L. McCrory, and R. L. Morse, Phys. Rev. Lett. 34, 721 (1975); R. A. Haas *et al.*, Phys. Fluids 20, 322 (1977); M. D. Rosen *et al.*, Phys. Fluids 22, 2020 (1979); W. C. Mead *et al.*, Phys. Rev. Lett. 47, 1289 (1981).

[3]J. A. Tarvin and R. J. Schroeder, Phys. Rev. Lett. 47, 341 (1981).

[4]L. Spitzer, Jr., *Physics of Fully Ionized Gases* (Wiley, New York, 1967).

[5]A. R. Bell, R. G. Evans, and D. J. Nicholas, Phys. Rev. Lett. 46, 243 (1981); R. J. Mason, Phys. Rev. Lett. 47, 652 (1981).

[6]F. C. Young *et al.*, Appl. Phys. Lett. 30, 45 (1977).

[7]B. Yaakobi and T. C. Bristow, Phys. Rev. Lett. 38, 350 (1977); B. H. Ripin *et al.*, Phys. Rev. Lett. 43, 350 (1979); B. H. Ripin *et al.*, Phys. Fluids 23, 1012 (1980); H. Nishimura *et al.*, Phys. Rev. A 23, 2011 (1981); Opt. Commun. 39, 175 (1981).

[8]F. Amiranoff *et al.*, Phys. Rev. Lett. 43, 522 (1979); R. Fabbro *et al.*, Phys. Rev. A 26, 2289 (1982).

[9]J. Grun, R. DeCoste, B. H. Ripin, and J. Gardner, Appl. Phys. Lett. 39, 545 (1981); J. Grun *et al.*, Phys. Fluids 26, 588 (1983).

[10]T. J. Goldsack, J. D. Kilkenny, and P. T. Rumsby, J. Phys. D 14, L47 (1981); T. J. Goldsack *et al.*, Phys. Fluids 25, 1634 (1982).

[11]B. Yaakobi *et al.*, "Laser Interaction and Related Plasma Phenomena, Vol. 6" (to be published).

[12]C. E. Max, C. F. McKee, and W. C. Mead, Phys. Fluids 23, 1620 (1980).

[13]C. E. Thomas and L. D. Siebert, Appl. Opt. 15, 462 (1976).

[14]C. J. Charnetski, Opt. Eng. 22, SR-012 (1983); KMS Fusion Annual Technical Report, 1981 (unpublished), Secs. 2.1.3 and 2.1.4.

[15]W. B. Fechner *et al.*, KMS Fusion Report No. U-1329 (to be published).

[16]J. D. Simpson, Rev. Sci. Instrum. 53, 1870 (1982).

[17]D. C. Slater *et al.*, Phys. Rev. Lett. 46, 1199 (1981).

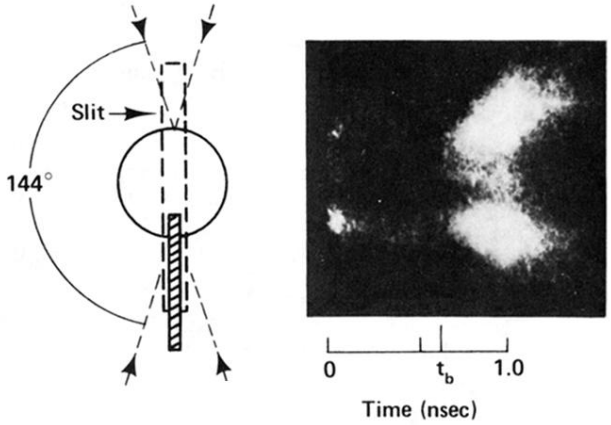

FIG. 1. X-ray streak photograph, showing the rapid increase of emission when the parylene has been ablated and the Al layer is heated. Note the short burst of x rays from the Ti layer, which marks the onset of the laser pulse. The sketch shows the target image produced by the pinhole camera superimposed on the slit-like photocathode. The marginal rays of the two 144° cones of laser light are also shown.